IEEE Access
Multidisciplinary | Rapid Review | Open Access Journal

Received December 25, 2019, accepted December 30, 2019, date of publication January 1, 2020, date of current version January 16, 2020.

*Digital Object Identifier 10.1109/ACCESS.2019.2963500*

# A DC Series Arc Fault Detection Method Using Line Current and Supply Voltage

**QIWEI LU, ZEYU YE, MENGMENG SU, YASONG LI, YUCE SUN, AND HANQING HUANG**

School of Mechanical Electronic and Information Engineering, China University of Mining and Technology, Beijing 100083, China

Corresponding author: Qiwei Lu (lqw@cumtb.edu.cn)

This work was supported by Shenhua Group Co., Ltd., Science and Technology Innovation under Project CSIE16024877.

**ABSTRACT** In recent years, DC fault arc detection has been an electrical engineering research hotspot. At present, most proposed detection methods do not analyze the effects of fault arc electrical characteristics on both line current and supply voltage. Therefore, this study extensively analyzes variations of the line current and supply voltage because of DC arc faults based on the volt-ampere characteristics of DC arc faults. Then, a DC series arc fault detection method is proposed that comprehensively uses information on line current and supply voltage. An experimental platform for DC fault arc generation and detection was established using a DC-DC converter and a photovoltaic power supply as DC power supplies, and the proposed method was confirmed by experiments using this platform. Experimental results demonstrate that the proposed method can effectively distinguish arc faults and has the characteristics of clear physical meaning while maintaining a low amount of calculation.

**INDEX TERMS** DC series arc, volt-ampere characteristic, electrical fault detection, current, voltage, chaotic characteristics, drop rate, change rate.

## I. INTRODUCTION

DC power has been extensively used in electric vehicles, data centers, and communication systems [1]–[3]. Multiple household loads, such as LED bulbs, television, printers, air conditioning, washing machines, and refrigerators internally operate on DC [4], [5]. Moreover, certain distributed renewable energy power generation systems, such as photovoltaic (PV) systems, are based on DC. Because DC power has the advantages of low line cost, low transmission loss, and high reliability [6], [7], many DC power distribution demonstration projects have been globally developed in recent years [8], [9]. Furthermore, China has developed a standard, known as GB/T 35727-2017 ''Guideline for standard voltage of medium and low voltage DC distribution system'' to widen the use of DC power [10]. Therefore, it is reasonable to expect that more applications of DC power will appear. In a DC power system, a fault arc may occur because of aging of electrical line insulation, loosening electrical connections, humid air, or a sharp voltage or current increase; DC fault arcs are an important factor in electrical fires. Therefore, examining DC fault arc detection technology is crucial to improve DC power safety. Currently, this study has become a hotspot in electrical engineering research.

Compared with AC systems, studies on DC arc fault detection technology started late. In 2011, UL published its DC arc fault detection standard, ''Standard for Photovoltaic (PV) DC Arc-Fault Circuit Protection'' (UL-1699B) [11]; however, the corresponding AC arc fault detection standard UL-1699 was published in 1999. Furthermore, there is no natural zero-crossing point in a DC power supply and DC arc faults are difficult to extinguish, thus, the DC arc faults possess considerable potential for harm compared to AC arc faults.

In an AC circuit, there will be different line current waveforms under different load types. Thus, when an arc fault occurs, the line current will generally have a flat shoulder at the line current's natural zero-crossing point; the line current's periodicity will be damaged, and the harmonic proportion of the line current will change. Therefore, load types can be identified by the line current's waveform, and the corresponding detection criteria can be selected based on that load type. However, DC circuit line current has no natural zero-crossing point; thus, the abovementioned phenomena no longer exist. Consequently, to detect DC arc faults, it is difficult to directly use most existing AC arc fault detection technologies [12]. Moreover, loads are basically equivalent to a resistor under a steady-state condition in DC circuits. If we

The associate editor coordinating the review of this manuscript and approving it for publication was Gerard-Andre Capolino.

only use line current characteristics, normal operations that occur as the load changes can be easily mistaken for arc faults, increasing the difficulty of detection.

Recently, researches have examined various DC arc fault characteristics and proposed certain detection methods. Existing DC arc fault detection methods primarily detect arc faults using the physical characteristics of arcs and the effect of arc resistance and its dynamic change to line current. Arc faults are accompanied by physical characteristics such as electromagnetic radiation, light, and noise. Methods based on such physical characteristics can thus be used to detect arc faults. In [13], DC arc fault electromagnetic radiation signal amplitude and frequency spectra are analyzed and a fault detection method based on electromagnetic radiation signal was proposed. Furthermore, the effects of electrode material, current, and pressure on arc fault electromagnetic radiation are further analyzed [14]. However, these methods can only detect arc faults at specific locations as the sensor's installation position is restricted.

An arc fault can be considered as a dynamic nonlinear resistance element in the circuit network. Its resistance is related to the arc's temperature, the supply voltage magnitude, electrode material, the surrounding gas composition, and the arc gap's spacing [15]. The abovementioned parameters are not always constant while the arc is burning, e.g., an arc will produce high temperature that causes the electrode to volatilize, which then affects the arc length. Perhaps arc length increases with time, it becomes prolonged. Arcs can be caused by loose connections, in which case the arc would cause the metal conductor to melt. Thus, the equivalent length of the arc could become shorter. Therefore, the arc's equivalent resistance varies randomly and irregularly, resulting in the line current's dynamic range showing chaotic characteristics [16], [17]. The irregular fluctuation of the line current in the time domain, and the specific frequency band amplitude in the frequency domain will both increase. Based on arc characteristics in specific application occasions, multiple DC fault arc detection methods have been proposed.

An arc fault detection algorithm based on modified Tsallis entropy using entropy to distinguish the chaotic and orderly variations of signals was proposed in [16]. In [17], current variation chaos was analyzed in both the time and time-frequency domains, and a series fault arc detecting methods using current variation and root mean square values of wavelet coefficients is proposed. In [18], a fast Fourier transform (FFT) is used to analyze line current spectrum characteristics, and a series fault arc is detected based on line current amplitude changes before and after a fault arc at a specific frequency. In [19], the characteristics of the random variation of the current in the arc and the volt-ampere (*V-I*) characteristics of a PV power supply are used to analyze the effects of the series fault arc on PV supply voltage. A DC series arc fault detection method using the PV supply voltage variance is proposed. In [20], arc resistance variation rapidity is used. The PV module output power, line current, and supply voltage are detected, and their rates of change are used as a basis for detecting a fault arc.

When a series arc fault occurs, it will generate an arc voltage on the arc gap. Because it is difficult to know an arc's location in advance, arc fault detection cannot be achieved by detecting arc voltage. However, arc voltage in the line affects both line current and load voltage. In [21], the effects of arc voltage on load voltage under different impedance parameters was analyzed, and DC series arc fault detection method based on the load side voltage decrease at arc initiation is proposed.

Because of normal operations, such as power starting and load switching, the line current signal may have similar effects as arc faults. Thus, additional research is required to avoid false positives that can be attributed to normal operations [14], [22].

Recently, some studies have used machine learning-based methods to detect arc faults. In [23], system voltage and current signal characteristics are extracted using a wavelet transform. These features are then classified using a support vector machine to achieve arc fault recognition. In [24], hidden Markov models are trained to extract fault arc features in the time and frequency domains and a DC series arc detection method based on the IntelArc system is proposed. In [25], a detection method based on a deep convolutional generative adversarial network that can solve decreasing detection accuracy because of differences between the original data and the actual situation is proposed. These machine learning-based methods currently require large volumes of high-quality sample data to achieve higher accuracy.

Based on arc *V-I* characteristics, this study analyzes fault arc effects on the average line current value and the effects of the line current's chaotic characteristics on the AC component of power supply voltage. Then, a DC series arc fault detection method based on the change rule of the line current's average value and chaotic characteristics and the change rule of the supply voltage's AC component is proposed. Compared with DC fault arc detection methods based only on the chaos of the line current variation, our proposed will be more accurate because of the addition of the average line current value change rule and supply voltage AC component. Thus, this method has greater accuracy. Moreover, because we avoid the use of machine learning and advanced filtering techniques, this method does not need many training sets and its amount of calculation is reduced.

## II. ANALYSIS OF ARC *V-I* CHARACTERISTICS EFFECTS ON LINE CURRENT

### A. ARC V-I CHARACTERISTICS EFFECTS ON THE AVERAGE VALUE OF THE LINE CURRENT UNDER DIFFERENT ARC GAPS

A series arc can be considered a dynamic nonlinear resistance, and the arc gap's length gap will affect its *V-I* characteristics. The earliest study on arc *V-I* characteristics is the Ayrton equation, which was proposed in 1902.

Existing arc *V-I* equations include the Steinmetz equation, Nottingham equation, Van and Wallington equation, and Paukert equation [26]. Because of the different purposes of these studies, the different equations have considerably differing application scopes. Among these equations, the Paukert arc *V-I* equation covers a wide range of voltages and currents and contains information on the arc gap's range. Arc current ranges from 0.3 A to 100 kA and the arc gap ranges from 1 to 200 mm. Thus, the Paukert equation can fit arc fault situations in most cases and is shown in (1).

$$V_{\text{arc}} = \frac{a}{I_{\text{arc}}^{b}} \tag{1}$$

The values of $a$ and $b$ depend on the arc gap's length and the line current's average value. Based on (1), numerous experiments were performed in [17] to obtain (2).

$$V_{\text{arc}} = \frac{20.19 + 21.05L}{I_{\text{arc}}^{0.1174+0.075L}} \tag{2}$$

where $L$ is the arc gap length, which ranges from 1 to 3 mm, and the value of current $I_{\text{arc}}$ ranges from 3 to 25 A. Using (2), it is easier to calculate the line current during arcing than equation (1).

When detecting DC series arc faults, the line current is typically of <25 A; thus, (2) can be used in most applications. The curves of *V-I* characteristics with different $L$ values are shown in Fig. 1.

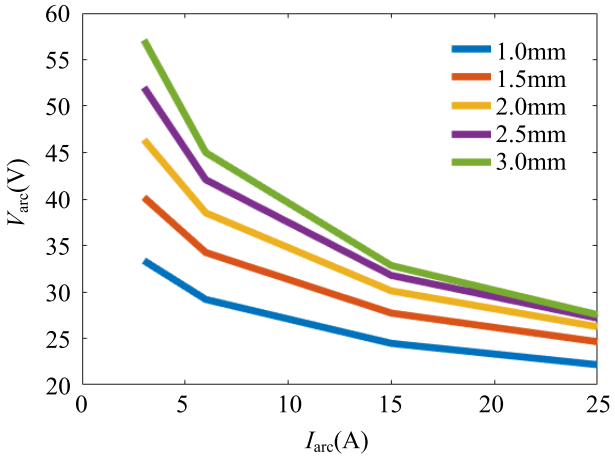


**FIGURE 1.** *V-I* curve under different arc gap lengths.

### 1) CONSTANT RESISTANCE LOAD

Because of the presence of arc voltage, the line current will be less than normal when an arc occurs. In the circuit shown in Fig. 2 where:

| | |
|---|---|
| $E$ | DC source voltage |
| $V_{\text{arc}}$ | arc voltage |
| $R_{\text{L}}$ | load resistance |
| $U_{\text{L}}$ | load voltage |
| $I_{\text{L}}$ | line current |

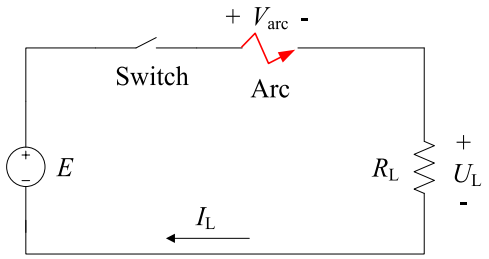


**FIGURE 2.** Simplified equivalent circuit for an arc experiment.

The line current $I_{\text{L}}$ before an arc occurs is as follows:

$$I_{\text{L}} = \frac{E}{R_{\text{L}}} \tag{3}$$

and when an arc occurs, the line current $I_{\text{L,arc}}$ is as follows:

$$I_{\text{L,arc}} = \frac{E - V_{\text{arc}}}{R_{\text{L}}} \tag{4}$$

From (3) and (4), when an arc fault occurs, the line current average value change rate $\eta$ can be expressed as follows:

$$\eta = \left| \frac{I_{\text{L}} - I_{\text{L,arc}}}{I_{\text{L}}} \right| = \frac{V_{\text{arc}}}{E} \tag{5}$$

By plugging (2) into (5), we obtain the following equation:

$$\eta = \frac{20.19 + 21.05L}{EI_{\text{arc}}^{0.1174+0.075L}} \tag{6}$$

where $V_{\text{arc}}$ increases with increased $L$ at the same current. Therefore, it can be seen from (6) that $\eta$ will increase as $L$ increases. Bringing the minimum (1 mm) and maximum (3 mm) values of $L$ into (6) yields the range of values of $\eta$.

$$\frac{41.23}{EI_{\text{L,arc}}^{0.20}} \le \eta \le \frac{83.33}{EI_{\text{L,arc}}^{0.34}} \tag{7}$$

Based on (7), $\eta$ at several typical line currents and supply voltages are shown in Tables 1 and 2 for $L$ values of 1 and 3 mm, respectively.

For example, for a supply voltage of 300 V and line current of 6 A, $\eta$ is 0.09 when $L$ is 1 mm and 0.15 when $L$ is 3 mm. If the range of $\eta$ calculated by (5) is between 0.09 and 0.15, an arc may occur in the line.

The line current may not be in the 3–25 A range and the arc gap may exceed 1–3 mm, e.g., under the arcing test conditions in UL-1699B, line current ranges 2.5–14 A and arc gap length ranges from 0.8 to 2.5 mm [11]. Moreover, equation (2) is fitted by experimental results, with an error of ∼10% [17]. To avoid misjudgment because of equation error, we multiply the results in Tables 1 and 2 by 0.8 and 1.2, respectively, to expand the scope of $\eta$. Based on the data in Tables 1 and 2, the range of $\eta$ for different supply voltages and line currents is shown in Table 3.

If $\eta$ is not in the range of Table 3, the change of the line current average is possibly not caused by an arc fault. When it is calculated by (5) that $\eta$ is within the range shown in Table 3 and an arc fault may occur. Thus, $\eta$ can be used as the basis for starting arc detection.

**TABLE 1.** $\eta$ of different supply voltages and line currents ($L$ = 1 mm).

| $E$(V) \ $I_{L,arc}$(A) | 3 | 6 | 15 | 25 |
|---|---|---|---|---|
| 100 | 0.32 | 0.28 | 0.24 | 0.22 |
| 300 | 0.11 | 0.09 | 0.08 | 0.07 |
| 800 | 0.03 | 0.03 | 0.03 | 0.02 |

**TABLE 2.** $\eta$ of different supply voltages and line currents ($L$ = 3 mm).

| $E$(V) \ $I_{L\_arc}$(A) | 3 | 6 | 15 | 25 |
|---|---|---|---|---|
| 100 | 0.58 | 0.46 | 0.34 | 0.28 |
| 300 | 0.20 | 0.15 | 0.11 | 0.10 |
| 800 | 0.08 | 0.06 | 0.05 | 0.04 |

**TABLE 3.** $\eta$ of different supply voltages and line currents.

| $E$(V) \ $I_{L,arc}$ (A) | 2–6 | 6–15 | 15–25 |
|---|---|---|---|
| 100–300 | 0.07–0.70 | 0.06–0.56 | 0.05–0.41 |
| 300–800 | 0.02–0.24 | 0.02–0.18 | 0.01–0.14 |

### 2) CONSTANT POWER LOAD

When the DC power load is a power electronic converter, it is equivalent to a constant power load. The input current of this load will increase with decreased input voltage. In this case:

Before an arc occurs:

$$I_{\mathrm{L}} = \frac{P_{\mathrm{L}}}{U_{\mathrm{L}}} = \frac{P_{\mathrm{L}}}{E} \tag{8}$$

When an arc occurs:

$$I_{\mathrm{L,arc}} = \frac{P_{\mathrm{L}}}{U_{\mathrm{L}}} = \frac{P_{\mathrm{L}}}{E - V_{\mathrm{arc}}} \tag{9}$$

From (8) and (9):

$$\eta = \left| \frac{I_{\mathrm{L}} - I_{\mathrm{L,arc}}}{I_{\mathrm{L}}} \right| = \frac{V_{\mathrm{arc}}}{E - V_{\mathrm{arc}}} \tag{10}$$

Plugging (2) into (9):

$$\eta = \frac{20.19 + 21.05L}{EI_{\mathrm{L,arc}}^{0.1174+0.075L} - 20.19 - 21.05L} \tag{11}$$

Equation (11) shows that $\eta$ will increase with increased $L$. Bringing the minimum and maximum values of $L$ (1 and 3 mm, respectively) into (11), we can obtain the range of $\eta$ values.

$$\frac{41.23}{EI_{\mathrm{L,arc}}^{0.20} - 41.23} \leq \eta \leq \frac{83.33}{EI_{\mathrm{L,arc}}^{0.34} - 83.33} \tag{12}$$

Based on (12), $\eta$ at several typical line currents and supply voltages when $L$ is 1 and 3 mm are shown in Tables 4 and 5, respectively.

**TABLE 4.** $\eta$ of different supply voltages and line currents ($L$ = 1 mm).

| $E$(V) \ $I_{L,arc}$(A) | 3 | 6 | 15 | 25 |
|---|---|---|---|---|
| 100 | 0.48 | 0.40 | 0.32 | 0.28 |
| 300 | 0.12 | 0.11 | 0.09 | 0.08 |
| 800 | 0.04 | 0.04 | 0.03 | 0.03 |

**TABLE 5.** $\eta$ of different supply voltages and line currents ($L$ = 3 mm).

| $E$(V) \ $I_{L\_arc}$(A) | 3 | 6 | 15 | 25 |
|---|---|---|---|---|
| 100 | 1.34 | 0.83 | 0.61 | 0.42 |
| 300 | 0.23 | 0.17 | 0.12 | 0.10 |
| 800 | 0.07 | 0.06 | 0.05 | 0.04 |

Similarly, the range of $\eta$ at several typical line currents and supply voltages under a constant power load can be obtained based on Tables 4 and 5 (Table 6).

**TABLE 6.** $\eta$ of different supply voltages and line currents.

| $E$(V) \ $I_{L,arc}$(A) | 2–6 | 6–15 | 15–25 |
|---|---|---|---|
| 100–300 | 0.09–1.60 | 0.07–0.99 | 0.06–0.73 |
| 300–800 | 0.03–0.28 | 0.02–0.20 | 0.02–0.14 |

To accurately detect DC arc, it is not sufficient to detect line current changes caused by arc faults. Moreover, it is necessary to analyze arc fault other characteristics' effects on the circuit.

## *B. EFFECT OF ARC V-I CHARACTERISTICS ON DYNAMIC CHANGE OF THE LINE CURRENT*

Based on the previous analysis, the arc faults will cause the average value of the line current change to be within a certain range. However, line current changes are not always caused by arc faults. Therefore, it is necessary to analyze line current changes because of other arc fault characteristics.

When the arc is burning, arc temperature, electrode material, and surrounding gas composition will be constantly changing. Furthermore, the electrode will locally volatilize, resulting in the dynamic gap length changes. Therefore, arc resistance will randomly fluctuate to a certain extent, causing a degree of randomness in the line current.

In [27], an arc model is established in which resistance is added as a random number varying over time. Therefore, when an arc fault occurs, if the DC voltage is constant, the line current can be considered to be random sequences. The random fluctuation of the line current in an arcing state has a degree of increase compared with the normal state.

We continuously sampled the line current's value and filtered out the line current's DC component. The line current's probability density distribution curve was obtained by fitting

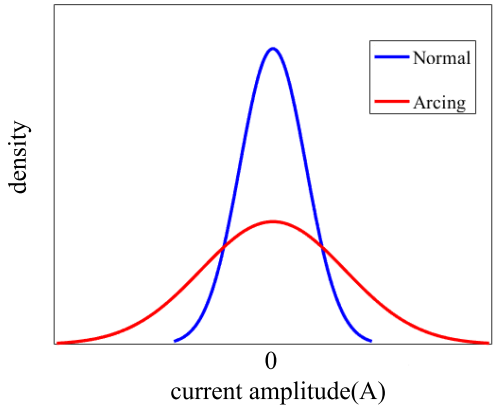


**FIGURE 3.** Probability density distribution of the line current.

the line current's AC component data. One study noted that the probability density distributions under normal and arcing states were very close to a normal distribution, as shown in Fig. 3 [28].

As seen in Fig. 3, the current distribution's probability density was considerably high near a current amplitude of 0. However, the current amplitude variation range in a normal state was smaller than that in an arcing state; thus, the probability density was much higher than that in an arcing state when the current amplitude was ∼0.

As shown in the distribution curve, the irregular line current fluctuation near the average value increased in an arcing state; thus the standard deviation was considerably higher than that in a normal state. The standard deviation's equation is shown in (13), where $x$ is a sequence with $N$ points.

$$X_{\text{std}} = \sqrt{\frac{1}{N}\sum_{i=1}^{N}(x_i - x_{\text{mean}})^2} \tag{13}$$

## III. ANALYSIS OF THE EFFECTS OF ARC *V-I* CHARACTERISTICS ON AC COMPONENT OF THE SUPPLY VOLTAGE

Line current in an arcing state shows a certain degree of chaos. This is because actual DC power supplies such as DC-DC converters and photovoltaic power supplies are not ideal voltage sources. The power supply's output voltage has an AC component; therefore, the change of the line current will affect the supply voltage change. In this section, we analyze the line current fluctuation's effect on the supply voltage's AC component.

### A. DC-DC CONVERTER

Fig. 4 shows a simplified circuit model considering a DC-DC converter's internal resistance.

where

$R_S$ internal resistance of the power supply
$R_L$ load resistance
$r$ arc resistance

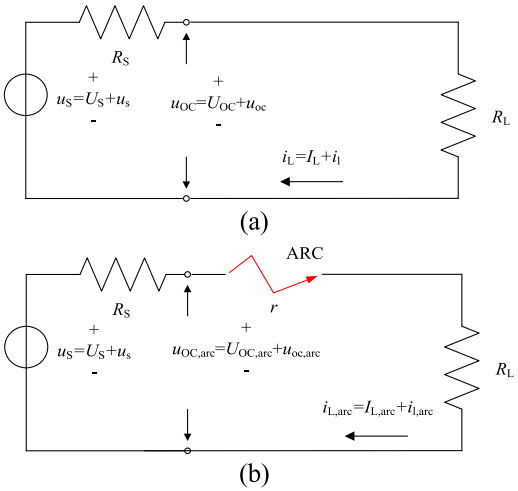


**FIGURE 4.** Simplified equivalent model of a DC power supply. (a) Normal state. (b) Arcing state.

$u_S$ voltage of an ideal voltage source
$U_S$ DC component of the voltage of an ideal voltage source
$u_s$ AC component of the voltage of an ideal voltage source
$u_{OC}$ output voltage
$U_{OC}$ DC component of the output voltage
$u_{oc}$ AC component of the output voltage
$i_L$ line current
$I_L$ DC component of the line current
$i_l$ AC component of the line current

In a normal state, $i_l$ is

$$i_l = \frac{u_s}{R_S + R_L} \tag{14}$$

and $u_{oc}$ is

$$u_{oc} = u_s\left(1 - \frac{R_S}{R_S + R_L}\right) \tag{15}$$

In Fig. 4b, $i_{l,arc}$ is as follows:

$$i_{l\_arc} = \frac{u_s}{R_S + R_L + r} \tag{16}$$

and $u_{oc,arc}$ is as follows:

$$u_{oc\_arc} = u_s\left(1 - \frac{R_S}{R_S + R_L + r}\right) \tag{17}$$

When series arc faults occur, $U_S$ will remain constant because of the control of the DC-DC converter feedback network. A comparison of (15) and (17) shows that the amplitude of $u_{oc,arc}$ will be considerably higher than that of $u_{oc}$ because of $r$ being in series in the line. Furthermore, the chaos of $u_{oc,arc}$ will increase because of the dynamic change of $r$.

If a wire in a practical circuit is longer, the line impedance cannot be ignored. Fig. 5 shows an equivalent circuit, where $R_0$ is the line resistance and $L_0$ is the line inductance. Here $L_0$ will affect the power supply's output voltage. When an

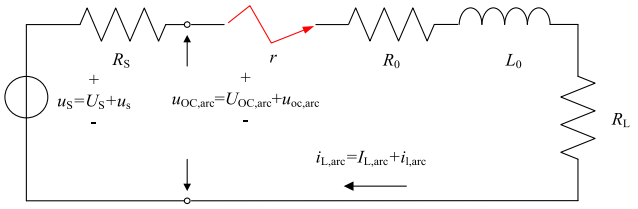


**FIGURE 5.** Simplified equivalent model of a DC power supply with a line impedance parameter.

arc occurs, the random dynamic change of the line current is intensified, the line current's high-frequency component increases, and d$i$/d$t$ increases. Therefore, the voltage on $L_0$ will be considerably higher than without arcing, and the amplitude of $u_{oc,arc}$ will increase further.

Therefore, regardless of whether the line impedance is considered, the amplitude of $u_{oc,arc}$ will increase when a fault arc occurs.

### B. PV POWER SUPPLY

Fig. 6 shows the equivalent model of a PV power supply [29]. It is assumed that the PV power supply's output power and internal resistance remain unchanged over a short time. The equivalent model can be simplified as shown in Fig. 4.

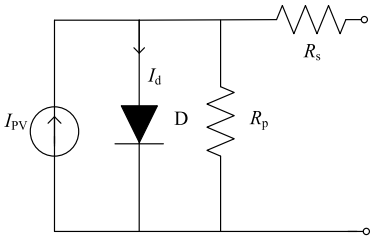


**FIGURE 6.** Equivalent model of a PV power supply.

The circuit model in a normal state is shown in Fig. 4a, and $i_l$ can be expressed as follows:

$$i_l = \frac{u_s}{R_S + R_L} \tag{18}$$

$R_L$ is the equivalent resistance of PV inverters. Because PV inverters are controlled by maximum power point tracking (MPPT) technology, $R_L$ is equal to $R_S$ when they operate at the maximum power point, and $i_l$ can be further expressed as follows:

$$i_l = \frac{u_s}{2R_S} \tag{19}$$

and $u_{oc}$ is as follows:

$$u_{oc} = \frac{u_s}{2} \tag{20}$$

If the MPPT control of PV inverters is fast enough in an arcing state, the $R_L$ is equal to $R_S + r$. Because the MPPT tracking speed is far less than the change speed of $r$, and $R_L$ is always in a constantly adjusting state, $i_{l,arc}$ is as follows:

$$i_{l,\,arc} = \frac{u_s}{R_S + R_L + r} \tag{21}$$

and $u_{oc,arc}$ is as follows:

$$u_{oc,arc} = u_s\left(1 - \frac{R_S}{R_S + R_L + r}\right) \tag{22}$$

Compared with (20) and (22), the amplitude of $u_{oc,arc}$ increases and fluctuates continuously because of the existence of the variable $r$. Because $R_L$ will always be in a constantly adjusting state rather than a stable value, the chaos of $u_{oc,arc}$ will increase.

For power electronic devices such as grid-connected PV inverters, the input is usually paralleled with a filter capacitor. Fig. 7 shows its equivalent circuit diagram. When there is a dynamically changing current because of an arc fault, it is necessary to consider the effect of $C_{in}$ on $u_{oc,arc}$.Because the AC impedance of $C_{in}$ is much smaller than that of $R_L$ under a high frequency current, most of the irregular dynamic current will pass through $C_{in}$ when an arc occurs and the $C_{in}$ will be charged. Thus, the voltage change rate of $C_{in}$ will be much larger. Under the same conditions, a smaller $C_{in}$ will yield a larger voltage change range on $C_{in}$. Therefore, when an arc fault occurs, the $C_{in}$ will increase the dynamic range of voltage, which will lead to an increased $u_{oc,arc}$.

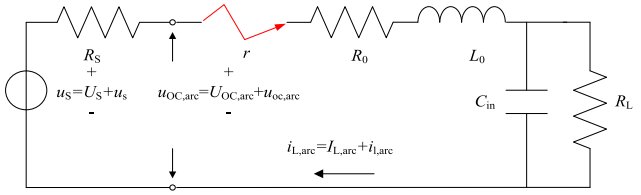


**FIGURE 7.** Simplified equivalent model of a DC power supply with a line impedance parameter and load capacitance.

Therefore, whether considering only $L_0$ or considering both $L_0$ and $C_{in}$, the $u_{oc,arc}$ is larger than $u_{oc}$ when an arc occurs. In fact, the value of $L_0$ is affected by the wire length and thickness and the value of $C_{in}$ is affected by the load type and load power. Although it is difficult to get accurate values of $L_0$ and $C_{in}$ in advance, these factors will increase $u_{oc,arc}$. Thus, the change of $u_{oc,arc}$ can be used as one of the characteristics to determine arc fault occurrence.

To summarize, whether a DC-DC converter or a PV power supply, arc resistance will lead to an increase in the amplitude and chaos of the output voltage's AC component. The AC components of the output voltage and line current change are primarily caused by the dynamic change of $r$; thus, if the changing trend is the same, the AC component of the output voltage can be calculated by the standard deviation.

## IV. DC SERIES ARC FAULT DETECTION METHOD

This section makes use of the line current drop, line current average change, and chaos of the line current and supply voltage to detect arc faults, and proposes a DC series arc fault detection method. Fig. 8 shows a flow chart of the proposed detection method.

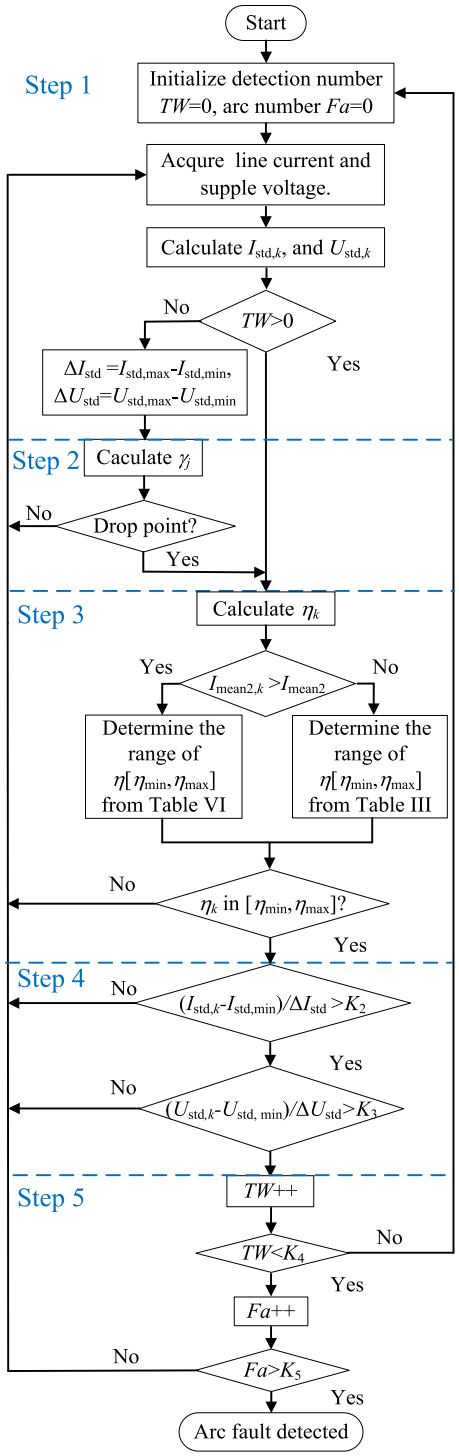


**FIGURE 8.** Detection flow chart.

Each step of the method is as follows:

1) Acquisition of line current and supply voltage signals: Acquire and store line current $i_L$ and supply voltage $u_S$ at regular intervals.
2) Calculation of the line current drop rate $\gamma$: Calculate the average value $I_{mean1}$ of consecutive $N$ current sampling points. If the sampling interval is $T_S$, this is equivalent to calculating the current average of a time window length $N^*T_S$. The difference $\gamma_j$, is then calculated as follows:

$$\gamma_j = I_{mean1,j} - I_{mean1,j+2} \tag{23}$$

$I_{mean1,j}$ and $I_{mean1,j+2}$ are the average line current values in the $j$th and $j+2$th time windows, respectively. Using the average value to calculate the drop rate can reduce noise interference, and calculating the drop rate between the $j$th and $j+2$th time windows can avoid error caused when the window crosses the drop point. If $\gamma_j$ is negative and meets the condition expressed in (24), the line current is considered to have dropped, which may be caused by arc faults.

$$\left|\frac{\gamma_{j+1}}{\gamma_j}\right| \geq K_1 \tag{24}$$

3) Calculation of the line current average value change rate $\eta$: Calculate the current average $I_{mean2}$ of a time window with a length of $M*T_S(M \gg N)$. The equation for $\eta_k$ can be expressed as follows.

$$\eta_k = \left|\frac{I_{mean2} - I_{mean2,k}}{I_{mean2}}\right| \tag{25}$$

where $I_{mean2,k}$ is the line current's average value in the $k$th time window and $I_{mean2}$ is the average value before the line current's drop point.

4) Calculation of the standard deviation: $I_{std,k}$ and $U_{std,k}$ are the standard deviations of the line current and AC component of the supply voltage in the $k$th time window, respectively. $\Delta I_{std}$ and $\Delta U_{std}$ are the ranges of standard deviation of the line current and AC component of the supply voltage in a normal state, respectively. $K_2$ and $K_3$ are the thresholds for measuring the degree of chaos in line current and AC component of the supply voltage, respectively.
5) Determining arc fault: When there are fault arcs in the $K_5$ time windows during the time of $K_4*M*T_S$, an arc fault detection signal is transmitted.

## V. EXPERIMENTS AND ANALYSIS

Based on the above analysis, we test the proposed detection method. An arc fault generator is established following the UL-1699B standard, with an arc generator connected in series in a circuit comprising a fixed electrode and a movable electrode, both of which are composed of copper. A DC-DC converter and PV supply are used as DC power supplies. We use a HIOKI6000 memory recorder to measure and record the line current and supply voltage, with a sampling frequency of 200 kHz.

### A. CONSTANT RESISTANCE LOAD

A DC-DC converter is used as the DC power supply in the test, and the load is constant resistance load. Fig. 9 shows the experimental platform. The low-voltage DC distribution voltage ranges from 176 to 231 V (nominal value is 220 V)

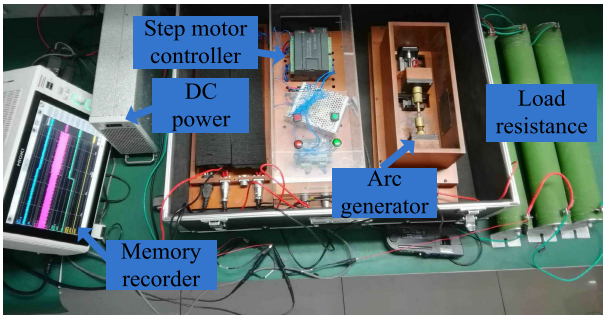


**FIGURE 9.** The experimental platform for series arc faults using a DC-DC converter as DC power supply.

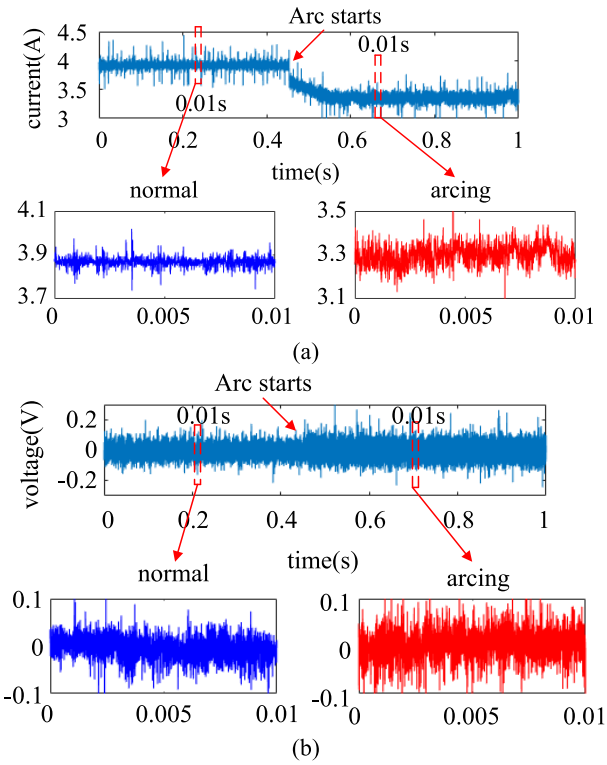


**FIGURE 10.** The experiment waveforms from normal state to arcing state under a constant resistance load (200 V/4 A). (a) Line current. (b) AC component of the supply voltage.

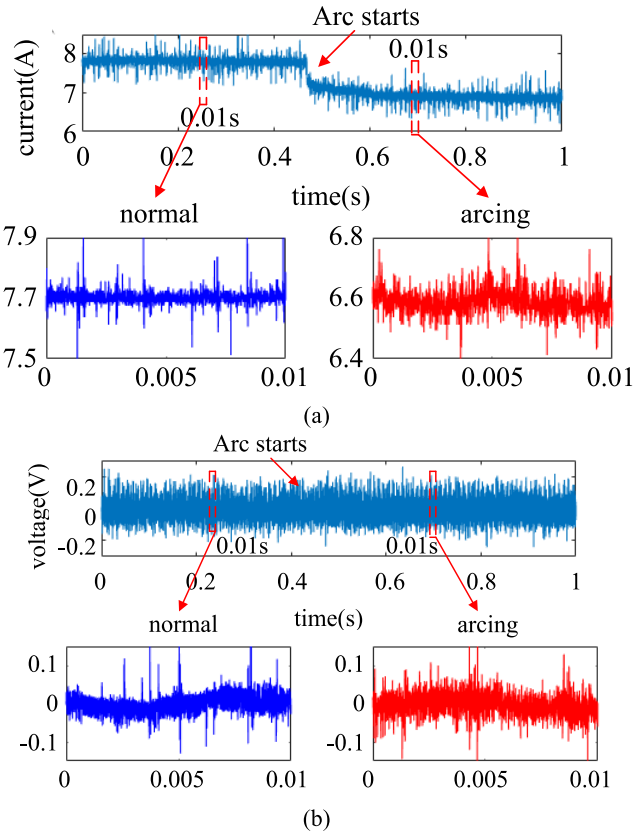


**FIGURE 11.** The experiment waveforms from normal state to arcing state under a constant resistance load (200 V/8 A). (a) Line current. (b) AC component of the supply voltage.

as dictated by the standard GB/T 35727-2017 [10], and the DC power supply voltage for the future telecommunications industry ranges from 260 to 400 V as recommended by the standard L.1200 [30]; thus, the supply voltage and line current are set to 200 V/4 A, 200 V/8 A and 330 V/12 A, respectively. The total length of the wire used in the experiment is 40 m. Based on UL-1699B, the line inductance parameter is 0.7 $\mu$H/m and the total line inductance is 28 $\mu$H. Figs. 10, 11, and 12 show the experiment waveforms.

### 1) LINE CURRENT DROP RATE

Considering 10 sampling points as a time window, we use (23) to calculate $\gamma$. At the arc starting point (ASP) in Figs. 10a, 11a, and 12a, $\gamma$ is 0.231 A, 0.322 A, and 0.473 A, respectively. During a normal state, the range of $\gamma$ is 0—0.071, 0–0.060, and 0–0.061 A, respectively. The $\gamma$ at the ASP is considerably higher than in a normal state. To provide additional evidence, the experiment was repeated 10 times, and the results are shown in Table 7.

**TABLE 7.** Experimental results of $\gamma$ for constant resistance loads.

| | 200V/4A | 200V/8A | 330V/12A |
|---|---|---|---|
| Normal state | 0–0.094 | 0–0.096 | 0–0.072 |
| ASP | 0.218–0.246 | 0.435–0.489 | 0.458–0.505 |

Units: (A)

As shown in Table 7, $\gamma$ at the ASP is more than twice as large as in a normal state. Therefore, $\gamma$ can be used as the basis for determining the drop point caused by an arc fault.

### 2) LINE CURRENT AVERAGE VALUE CHANGE RATE

When a drop point in the line current is detected, considering 10,000 sampling points (0.05 s) as time window length, the $\eta$ after ASP is calculated using (25). The range of $\eta$ in Fig. 10a is 0.13−0.16, that in Fig. 11a is 0.14−0.16, and that

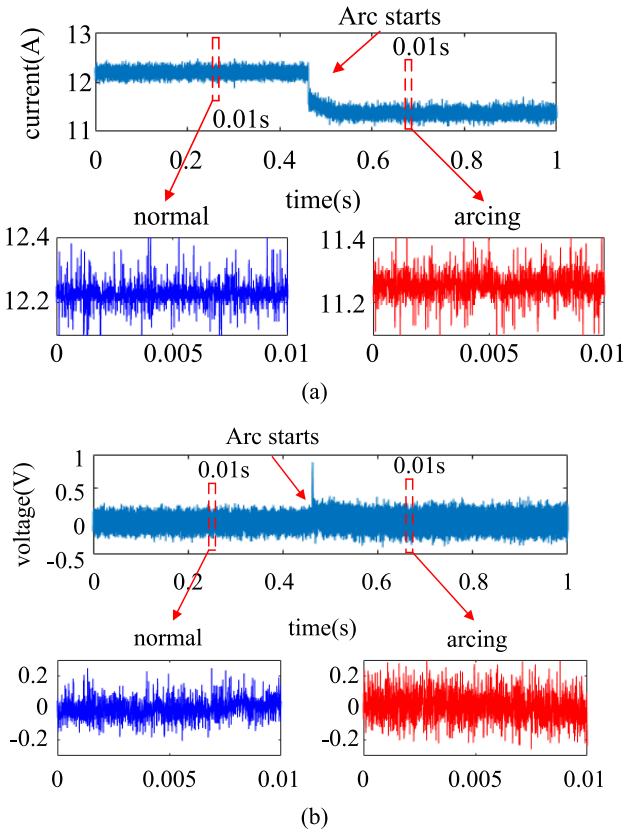


**FIGURE 12.** The experiment waveforms from normal state to arcing state under a constant resistance load (330 V/12 A). (a) Line current. (b) AC component of the supply voltage.

in Fig. 12a is 0.07–0.09. Thus, they are all within the range shown in Table 3.

Ten more experiments were conducted under the same conditions, and the results and corresponding ranges of $\eta$ from Table 3 are listed in Table 8. The range of experimental results of $\eta$ is within the range shown in Table 3. The experimental results show that the theoretical analysis in Section II is correct. Whether $\eta$ is within the range shown in Table 3, it can be used as a feature to determine whether an arc fault occurs.

**TABLE 8.** A comparison of the ranges of $\eta$ of a constant resistance load.

| | 200V/4A | 200V/8A | 330V/12A |
|---|---|---|---|
| From Table III | 0.07–0.70 | 0.06–0.56 | 0.02–0.18 |
| Experimental results | 0.13–0.17 | 0.12–0.16 | 0.06–0.09 |

### 3) STANDARD DEVIATION OF THE LINE CURRENT AND AC COMPONENT OF THE SUPPLY VOLTAGE

We selected 0.05 s as the time window length and used (13) to calculate the standard deviations of the data shown in Figs. 10, 11, and 12. The standard deviations of the line current in normal and arcing states are shown in Table 9. The standard deviation of the supply voltage's ac component in normal and arcing states is shown in Table 10.

**TABLE 9.** Standard deviations of the line currents for constant resistance loads.

| | 200V/4A | 200V/8A | 330V/12A |
|---|---|---|---|
| $I_{std,k}$(normal) | 0.021–0.023 | 0.025–0.031 | 0.033–0.035 |
| $\Delta I_{std}$ (normal) | 0.002 | 0.006 | 0.002 |
| $I_{std,k}$(arcing) | 0.038–0.043 | 0.045–0.059 | 0.040–0.046 |
| $I_{std,k}$-$I_{std,min}$(arcing) | 0.017–0.022 | 0.020–0.034 | 0.007–0.013 |

$I_{std,min}$ =min{ $I_{std,k}$ }; $I_{std,max}$ =max{ $I_{std,k}$ }; $\Delta I_{std}$ =$I_{std,max}$ -$I_{std,min}$

**TABLE 10.** Standard deviations of the AC component of the supply voltage for constant resistance loads.

| | 200V/4A | 200V/8A | 330V/12A |
|---|---|---|---|
| $U_{std,k}$ (normal) | 0.025–0.26 | 0.026–0.027 | 0.061–0.063 |
| $\Delta U_{std}$ (normal) | 0.001 | 0.001 | 0.002 |
| $U_{std,k}$(arcing) | 0.034–0.038 | 0.031–0.034 | 0.084–0.095 |
| $U_{std,k}$-$U_{std,min}$(arcing) | 0.009–0.013 | 0.005–0.008 | 0.023–0.034 |

$U_{std,min}$ =min{ $U_{std,k}$ }; $U_{std,max}$ =max{ $U_{std,k}$ }; $\Delta U_{std}$ =$U_{std,max}$ -$U_{std,min}$

Although $I_{std,k}$ and $U_{std,k}$ are larger in an arcing state than in a normal state, the difference is not large enough to easily set a threshold. However, the differences between $\Delta I_{std}$ and $I_{std,k}$-$I_{std,min}$ and $\Delta U_{std}$ and $U_{std,k}$-$U_{std,min}$ are obvious. Therefore, thresholds $K_2$ and $K_3$ can be easily set.

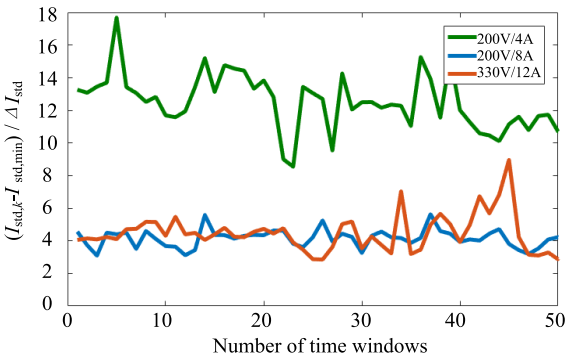


**FIGURE 13.** Values of ($I_{std,k}$-$I_{std,min}$)/$\Delta I_{std}$ of all experimental results for a constant resistance load.

To demonstrate that the proposed method can more easily determine the threshold, we conducted 10 experiments under the experimental conditions shown in Figs. 10, 11, and 12. We Selected $I_L$ and $U_S$ Values for five time windows in normal and arcing states to calculate ($I_{std,k}$-$I_{std,min}$)/$\Delta I_{std}$ and ($U_{std,k}$-$U_{std,min}$)/$\Delta U_{std}$. The values of ($I_{std,k}$-$I_{std,min}$)/$\Delta I_{std}$ are shown in Fig. 13, and the values of ($U_{std,k}$-$U_{std,min}$)/$\Delta U_{std}$ are shown in Fig. 14. These results demonstrate that all experimental results under the three conditions are higher than 2; thus, the threshold is easy to set.

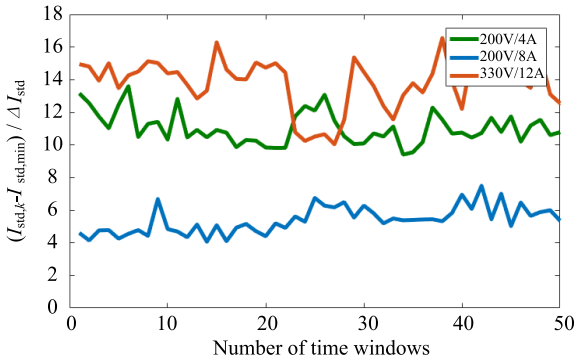


**FIGURE 14.** Values of $(U_{std,k}-U_{std,min})/\Delta U_{std}$ of all experimental results for a constant resistance load.

### B. CONSTANT POWER LOAD

If the DC load is from a power electronic device, it will show constant power characteristics. When the input voltage changes within a certain range, the output voltage will not change and the input current will change in the opposite direction.

The experiment circuit for a constant power load is shown in Fig. 15, and the experiment waveforms are shown in Fig. 16.

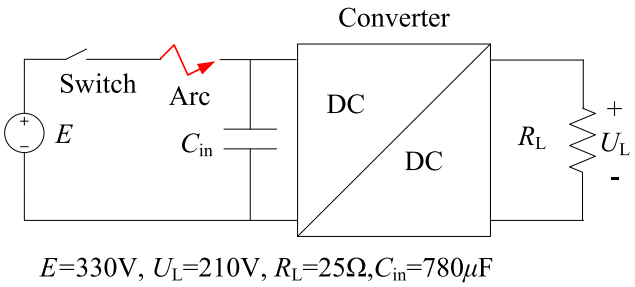


$E$=330V, $U_L$=210V, $R_L$=25Ω,$C_{in}$=780$\mu$F

**FIGURE 15.** Experiment circuit for a constant power load.

#### 1) LINE CURRENT DROP RATE

As shown in Fig. 16a, the line current will increase after an arc starts if the load is a constant power load; however, the line current will still drop at the moment the arc occurs.

At the ASP, the $\gamma$ value is 1.827 A, and the range of $\gamma$ during the normal state is 0.012–0.562 A. The $\gamma$ at the ASP is more than twice as large as $\gamma$ during the normal state; therefore, $\gamma$ can be used as the basis to determine the drop point caused by an arc fault.

When an arc fault occurs, the DC-DC converter's input voltage will decrease and its output power will remain constant; therefore, the input current will increase. However, when arcing occurs, the arc is equivalent to an additional resistor in the circuit, and the DC-DC converter controller will have not yet been adjusted. Therefore, $\gamma$ will increase suddenly when an arc fault occurs.

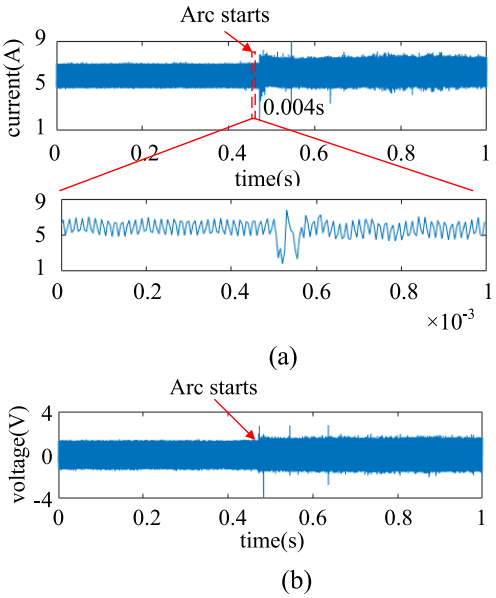


**FIGURE 16.** The experiment waveforms from normal state to arcing state under a constant power load. (b) AC component of the supply voltage.

#### 2) LINE CURRENT AVERAGE VALUE CHANGE RATE

In Fig. 16a, the $\eta$ values range from 0.04 to 0.12. Under this condition (line current of 6–15A and supply voltage of 300–800 V), the range of $\eta$ shown in Table 6 is 0.02–0.20. Thus, the $\eta$ in the experiment is within the range shown in Table 6.

#### 3) STANDARD DEVIATION OF THE LINE CURRENT AND AC COMPONENT OF THE SUPPLY VOLTAGE

Because each time window is set to 0.05 s and the sampling frequency is 200 KHz, the sampling number for each time window is 10K. The standard deviation of the data in each time window in Fig. 16 were calculated using (13). The standard deviation of the line current in Fig. 16a is shown in Table 11, and the standard deviation of the line current in Fig. 16b is shown in table 12.

**TABLE 11.** Standard deviation of the line current for a constant power load.

| | |
|---|---|
| $I_{std}$(normal) | 0.694–0.696 |
| $\Delta I_{std}$ (normal) | 0.002 |
| $I_{std,k}$(arcing) | 0.801–0.826 |
| $I_{std,k}$-$I_{std,min}$(normal) | 0.107–0.130 |

$I_{std,min}$ =min{ $I_{std,k}$ }; $I_{std,max}$ =max{ $I_{std,k}$ }; $\Delta I_{std}$ =$I_{std,max}$ -$I_{std,min}$

**TABLE 12.** Standard deviation of AC component of the supply voltage for a constant power load.

| | |
|---|---|
| $U_{std}$(normal) | 0.729–0.733 |
| $\Delta U_{std}$ (normal) | 0.004 |
| $U_{std,k}$(arcing) | 0.838–0.855 |
| $U_{std,k}$-$U_{std,min}$(normal) | 0.109–0.122 |

$U_{std,min}$ =min{ $U_{std,k}$ }; $U_{std,max}$ =max{ $U_{std,k}$ }; $\Delta U_{std}$ =$U_{std,max}$ -$U_{std,min}$

As shown in Tables 11 and 12, $I_{\text{std},k}$-$I_{\text{std,min}}$ ($U_{\text{std},k}$-$U_{\text{std,min}}$) is considerably higher than $\Delta I_{\text{std}}$($\Delta U_{\text{std}}$) under a constant power load. This is consistent with the theoretical analysis in Sections II and III. Because the chaotic characteristics obviously increase when an arc fault occurs, it is easy to set the threshold and thus detect the arc fault.

If the power of the load is constant, Γ will be higher than that in a normal state, and the chaotic characteristics of the line current and supply voltage will increase. The abovementioned two characteristics are the same as those for a constant resistance load. The difference is that the line current's average value will increase after the arc becomes stable.

### C. PV POWER SUPPLY

The experimental platform for DC series arc fault tests in a PV system is shown in Fig. 17. Eighteen solar panels are connected in series to form a grid-connected PV system. Each solar panel has a rated output power of 275 W, with a rated voltage of 31.0V and a rated current of 8.9 A. The grid-tied inverter model is a Growatt 10000 TL3-S, which has a DC input voltage range of 160—1000 VDC, a full-load MPPT voltage range of 450–850 VDC, and an AC rated output of 10 kW.

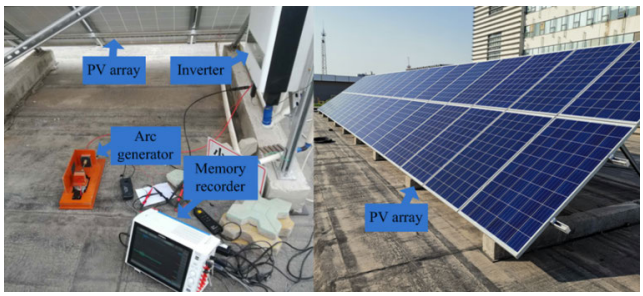


**FIGURE 17.** PV grid-connected experimental platform.

The experiment was conducted in Beijing on April 28, 2019. The day was cloudy with temperatures ranging from 9 to 20°. During the experiment, the supply voltage was ∼550 V and the line current is ∼2.6 A. Fig. 18 shows the experimental.

#### 1) LINE CURRENT DROP RATE

Considering 10 sampling points as a time window, (23) is used to calculate $\gamma$. At the ASP in Fig. 18a, $\gamma$ is 0.106 A, and the range of $\gamma$ is 0–0.020 A during a normal state.

Ten experiments were conducted, and the results of those experiments are shown in Table 13.

As shown in Table 13, the $\gamma$ value at the ASP is more than twice as large as in the normal state. Therefore, $\gamma$ can be used as the basis for determining the drop point caused by an arc fault.

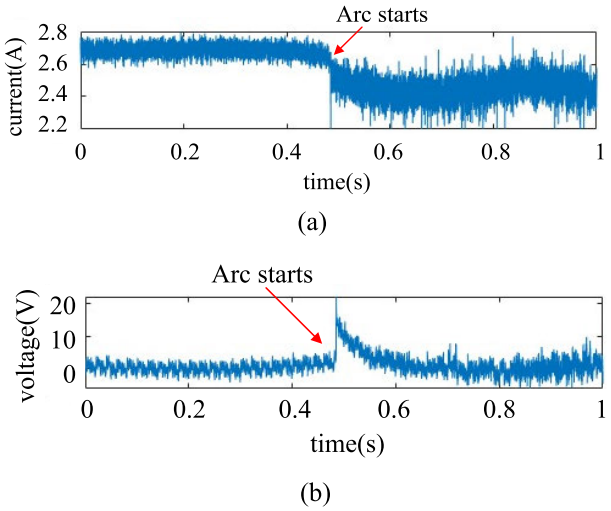


**FIGURE 18.** The experiment waveforms from normal state to arcing state in a grid-connected system. (a) Line current. (b) AC component of the supply voltage.

**TABLE 13.** Experimental results of $\gamma$ for a PV power supply.

| | $\gamma$(A) |
|---|---|
| Normal state | 0 - 0.031 |
| ASP | 0.079 - 0.254 |

#### 2) LINE CURRENT AVERAGE VALUE CHANGE RATE

Considering 10,000 sampling points (0.05 s) as the time window length, the experimental results of $\eta$ in Fig. 18a range from 0.06 to 0.08. When the line current is 2–6 A and the supply voltage is 300–800 V, the range of $\eta$ shown in Table 3 is 0.02–0.24.

Ten more experiments were conducted under the same conditions, and the range of $\eta$ shown in Table 3 is compared with the range of experimental results, as shown in Table 14.

**TABLE 14.** A comparison of the range of $\eta$ for a PV power supply.

| | range of $\eta$ |
|---|---|
| From Table III | 0.02 - 0.24 |
| Experimental results | 0.03 - 0.08 |

As shown in Table 14, the experimental results of $\eta$ are all within the range listed in.

#### 3) STANDARD DEVIATION OF THE LINE CURRENT AND AC COMPONENT OF THE SUPPLY VOLTAGE

We selected 0.05 s as the time window length to calculate the standard deviation of the data in Fig. 18. Table 15 shows the standard deviations of line currents in normal and arcing.

**TABLE 15.** Standard deviations of the PV power supply line current.

| | |
|---|---|
| $I_{std}$(normal) | 0.016–0.020 |
| $\Delta I_{std}$ (normal) | 0.004 |
| $I_{std,k}$(arcing) | 0.035–0.052 |
| $I_{std,k}$-$I_{std,min}$(normal) | 0.019–0.036 |

$I_{std,min}$ =min{ $I_{std,k}$ }; $I_{std,max}$ =max{ $I_{std,k}$ }; $\Delta I_{std}$ =$I_{std,max}$ -$I_{std,min}$

**TABLE 16.** Standard deviation of AC component of the PV power supply voltage.

| | |
|---|---|
| $U_{std}$(normal) | 1.27–1.39 |
| $\Delta U_{std}$ (normal) | 0.12 |
| $U_{std,k}$(arcing) | 1.78–2.24 |
| $U_{std,k}$-$U_{std,min}$(normal) | 0.51–0.97 |

$U_{std,min}$ =min{ $U_{std,k}$ }; $U_{std,max}$ =max{ $U_{std,k}$ }; $\Delta U_{std}$ =$U_{std,max}$ -$U_{std,min}$

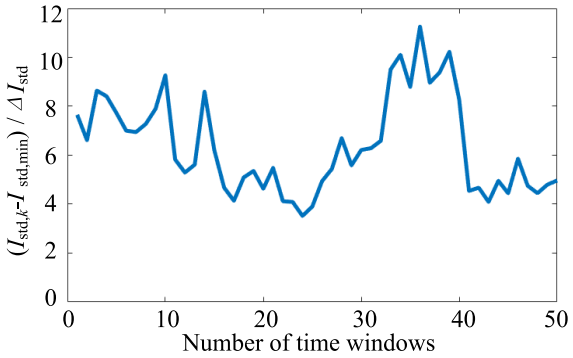


**FIGURE 19.** Values of $(I_{std,k}\text{-}I_{std,min})/\Delta I_{std}$ for all experimental results of a PV power supply.

The standard deviations of the AC component of the supply voltage in normal and arcing states are shown in Table 16.

As shown in Tables 15 and 16, compared with $I_{std,k}(U_{std,k})$ in normal and arcing states, the differences between $I_{std,k}$-$I_{std,min}$ and $\Delta I_{std}$ ($U_{std,k}$-$U_{std,min}$ and $\Delta U_{std}$) are more obvious.

Ten experiments were repeated with the PV system. The values of $(I_{std,k}\text{-}I_{std,min})/\Delta I_{std}$ are shown in Fig. 19, and the values of $(U_{std,k}\text{-}U_{std,min})/\Delta U_{std}$ are shown in Fig. 20.

As shown in Figs. 19 and 20, the experimental results in all three cases are greater than 2. Thus, The Threshold Is Easy To Determine.

To summarize, the proposed method can effectively detect DC series arc faults. Determining the line current drop point is a key step in this method's approach. If the threshold $K_1$ is set too high, the line current drop point may be missed, which would cause the arc fault detection procedure to fail. Thus, it would be better to set the threshold $K_1$ to a relatively small value if the arc detection method is started in a normal state. Because it cannot meet other arc fault detection criteria, it would not lead to misjudgment. Distinguishing between ''good'' and ''bad'' arcs in applications is crucial to avoid unnecessary tripping. In the proposed detection method, a value of fa that is greater than K5 indicates that

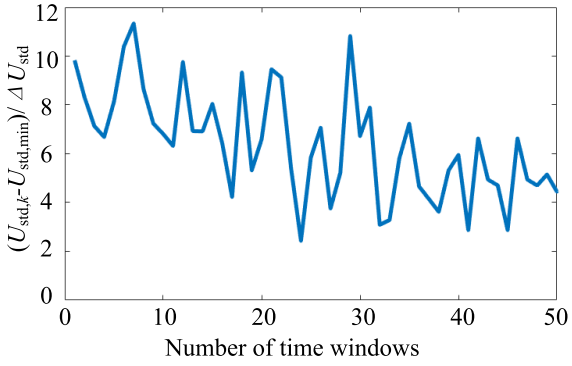


**FIGURE 20.** Values of $(U_{std,k}\text{-}U_{std,min})/\Delta U_{std}$ for all experimental results of a PV power supply.

there are more than K5 time windows in which an arc occurs within K4*0.05s. Thus, an arc fault (''bad'' arc) is considered to have occurred. because ''good'' arcs generally last a shorter time than ''bad'' arcs, setting a reasonable value of K5 can reduce or avoid the possibility of misjudging ''good'' arcs as ''bad'' arcs.

## VI. CONCLUSION

Based on the DC arc's *V-I* characteristics, changes in the line current and AC component of the supply voltage when arc faults occur are analyzed, and a method for detecting DC series fault arcs. This method detects DC series arc faults by detecting line current drops, line current average value change rates, and the standard deviations of the line current and the ac component of the supply voltage. A DC-DC converter and a PV power supply are used as DC power supplies for experimental verification.

Compared with frequency spectrum analysis of the line current, the proposed method avoids FFT or wavelet transforms of the line current and reduces the amount of calculation. furthermore, compared with machine learning methods, the proposed method does not need much data to learn. Thus, the proposed method is simpler and easier to implement using a low-cost single-chip computer.

## REFERENCES

[1] H. Chen, H. Kim, R. Erickson, and D. Maksimovic, "Electrified automotive powertrain architecture using composite DC–DC converters," *IEEE Trans. Power Electron.*, vol. 32, no. 1, pp. 98–116, Jan. 2017.

[2] P. Das, M. Pahlevaninezhad, and A. K. Singh, "A novel load adaptive ZVS auxiliary circuit for PWM three–level DC–DC converters," *IEEE Trans. Power Electron.*, vol. 30, no. 4, pp. 2108–2126, Apr. 2015.

[3] C. Li, Y. Zhong, and D. Xu, "Soft-switching three-phase matrix based isolated AC–DC converter for DC distribution system," in *Proc. IEEE Energy Convers. Congr. Expo. (ECCE)*, Montreal, QC, Canada, Sep. 2015, pp. 6755–6761.

[4] N. C. Sahoo, S. Mohapatro, A. K. Sahu, and B. S. Mohapatro, "Loss and cost evaluation of typical DC distribution for residential house," in *Proc. IEEE Int. Conf. Power Energy (PECon)*, Melaka, Malaysia, Nov. 2016, pp. 668–673.

[5] F. Zhang, C. Meng, Y. Yang, C. Sun, C. Ji, Y. Chen, W. Wei, H. Qiu, and G. Yang, "Advantages and challenges of DC microgrid for commercial building a case study from Xiamen University DC microgrid," in *Proc. IEEE 1st Int. Conf. DC Microgrids (ICDCM)*, Atlanta, GA, USA, Jun. 2015, pp. 355–358.

[6] M. Starke, L. M. Tolbert, and B. Ozpineci, "AC vs. DC distribution: A loss comparison," in *Proc. IEEE/PES Transmiss. Distrib. Conf. Expo.*, Chicago, IL, USA, Apr. 2008, pp. 1–7.
[7] F. Wang, Y. Pei, D. Boroyevich, R. Burgos, and K. Ngo, "Ac vs. DC distribution for off-shore power delivery," in *Proc. 34th Annu. Conf. IEEE Ind. Electron.*, Orlando, FL, USA, Nov. 2008, pp. 2113–2118.
[8] C. Zhao, C. Gu, F. Li, and M. Dale, "Understanding LV network voltage distribution- UK smart grid demonstration experience," in *Proc. IEEE Power Energy Soc. Innov. Smart Grid Technol. Conf. (ISGT)*, Washington, DC, USA, Feb. 2015, pp. 1–5.
[9] T. Taufik and M. Muscarella, "Development of DC house prototypes as demonstration sites for an alternate solution to rural electrification," in *Proc. 6th Int. Annu. Eng. Seminar (InAES)*, Yogyakarta, Indonesia, Aug. 2016, pp. 262–265.
[10] *Guideline for Standard Voltages of Medium and Low Voltage DC Distribution System*, Standard GB/T 35727-2017, 2017.
[11] *Standard for Photovoltaic (PV) DC Arc-Fault Circuit Protection*, Standard UL 1699B, Underwriters Laboratories, Northbrook, IL, USA, Aug. 2018.
[12] X. Yao, L. Herrera, L. Yue, and H. Cai, "Experimental study of series DC arc in distribution systems," in *Proc. IEEE Energy Convers. Congr. Expo. (ECCE)*, Portland, OR, USA, Sep. 2018, pp. 3713–3718.
[13] Q. Xiong, S. Ji, L. Zhu, L. Zhong, and Y. Liu, "A novel DC arc fault detection method based on electromagnetic radiation signal," *IEEE Trans. Plasma Sci.*, vol. 45, no. 3, pp. 472–478, Mar. 2017.
[14] Q. Xiong, S. Ji, X. Liu, X. Li, L. Zhu, X. Feng, A. L. Gattozzi, and R. E. Hebner, "Electromagnetic radiation characteristics of series DC arc fault and its determining factors," *IEEE Trans. Plasma Sci.*, vol. 46, no. 11, pp. 4028–4036, Nov. 2018.
[15] A. Khakpour, S. Franke, D. Uhrlandt, S. Gorchakov, and R.-P. Methling, "Electrical arc model based on physical parameters and power calculation," *IEEE Trans. Plasma Sci.*, vol. 43, no. 8, pp. 2721–2729, Aug. 2015.
[16] N. L. Georgijevic, M. V. Jankovic, S. Srdic, and Z. Radakovic, "The detection of series arc fault in PV systems based on the arc current entropy," *IEEE Trans. Power Electron.*, vol. 31, no. 8, pp. 5917–5930, Aug. 2016.
[17] X. Yao, L. Herrera, S. Ji, K. Zou, and J. Wang, "Characteristic study and time-domain discrete-wavelet–transform based hybrid detection of series DC arc faults," *IEEE Trans. Power Electron.*, vol. 29, no. 6, pp. 3103–3115, Jun. 2014.
[18] S. Chae, J. Park, and S. Oh, "Series DC arc fault detection algorithm for DC microgrids using relative magnitude comparison," *IEEE J. Emerg. Sel. Topics Power Electron.*, vol. 4, no. 4, pp. 1270–1278, Dec. 2016.
[19] F. Schimpf and L. E. Norum, "Recognition of electric arcing in the DC-wiring of photovoltaic systems," in *Proc. 31st Int. Telecommun. Energy Conf. (INTELEC)*, Incheon, South Korea, Oct. 2009, pp. 1–6.
[20] M. Dargatz and M. Fomage, "Method and apparatus for detection and control of DC arc faults," U.S. Patent 8 179 147, May 15, 2012.
[21] A. Shekhar, L. Ramirez-Elizondo, S. Bandyopadhyay, L. Mackay, and P. Bauera, "Detection of series arcs using load side voltage drop for protection of low voltage DC systems," *IEEE Trans. Smart Grid*, vol. 9, no. 6, pp. 6288–6297, Nov. 2018.
[22] Y.-S. Oh, J. Han, G.-H. Gwon, D.-U. Kim, and C.-H. Kim, "Development of fault detector for series arc fault in low voltage DC distribution system using wavelet singular value decomposition and state diagram," *J. Elect. Eng. Technol.*, vol. 10, no. 3, pp. 766–776, May 2015.
[23] Z. Wang and R. S. Balog, "Arc fault and flash detection in photovoltaic systems using wavelet transform and support vector machines," in *Proc. IEEE 43rd Photovolt. Spec. Conf. (PVSC)*, Portland, OR, USA, Jun. 2016, pp. 3275–3280.
[24] R. D. Telford, S. Galloway, B. Stephen, and I. Elders, "Diagnosis of series DC arc faults—A machine learning approach," *IEEE Trans. Ind. Informat.*, vol. 13, no. 4, pp. 1598–1609, Aug. 2017.
[25] S. Lu, T. Sirojan, B. T. Phung, D. Zhang, and E. Ambikairajah, "DA–DCGAN: An effective methodology for DC series arc fault diagnosis in photovoltaic systems," *IEEE Access*, vol. 7, pp. 45831–45840, 2019.
[26] R. F. Ammerman, T. Gammon, P. K. Sen, and J. P. Nelson, "DC–arc models and incident–energy calculations," *IEEE Trans. Ind. Appl.*, vol. 46, no. 5, pp. 1810–1819, Sep. 2010.
[27] F. M. Uriarte, A. L. Gattozzi, J. D. Herbst, H. B. Estes, T. J. Hotz, A. Kwasinski, and R. E. Hebner, "A DC arc model for series faults in low voltage microgrids," *IEEE Trans. Smart Grid*, vol. 3, no. 4, pp. 2063–2070, Dec. 2012.
[28] X. Yao, L. Herrera, and J. Wang, "Impact evaluation of series DC arc faults in DC microgrids," in *Proc. IEEE Appl. Power Electron. Conf. Expo. (APEC)*, Charlotte, NC, USA, Mar. 2015, pp. 2953–2958.
[29] H. M. Hasanien, "Shuffled frog leaping algorithm for photovoltaic model identification," *IEEE Trans. Sustain. Energy*, vol. 6, no. 2, pp. 509–515, Apr. 2015.
[30] *Direct Current Power Feeding Interface Up to 400 V at the Input to Telecommunication and ICT Equipment*, Standard L.1200, International Telecommunication Union, Geneva, Switzerland, 2012.

**QIWEI LU** was born in Shijiazhuang, Hebei, China, in 1976. He was a Visiting Scholar with the Department of Electrical and Computer Engineering, North Carolina State University, USA, in 2014. He is currently the Director of the Department of Electrical Engineering and an Adjunct Professor with the China University of Mining and Technology, Beijing. He has published over 30 articles in peer-reviewed journals and conferences. His research interests include solid state circuit breaker, fault arc detection and protection, and energy saving of train.

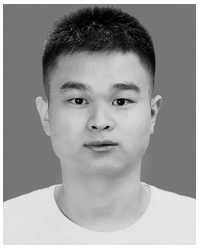

**ZEYU YE** was born in Huainan, China, in 1995. He received the B.S. degree in electrical engineering from the Anhui University of Science and Technology, Huainan, China, in 2017. He is currently pursuing the M.S. degree with the China University of Mining and Technology, Beijing, China. His current research interests include features and the detection of arc fault.

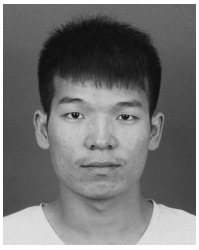

**MENGMENG SU** was born in Bozhou, China, in 1995. He received the B.S. degree in electrical engineering from the China University of Mining and Technology, Beijing, China, in 2018, where he is currently pursuing the master's degree. His current research interests include dc arc fault detection and artificial intelligence applications for electrical engineering.

**YASONG LI** was born in Yuncheng, China, in 1997. He received the B.S. degree in electrical engineering from the China University of Mining and Technology, Beijing, China, in 2019, where he is currently pursuing the master's degree. His current research interest includes dc arc fault detection.

**YUCE SUN** was born in Shijiazhuang, China, in 1999. He is currently pursuing the degree in electrical engineering with the China University of Mining and Technology, Beijing, China. His current research interests include dc arc fault detection and artificial intelligence applications for electrical engineering.

**HANQING HUANG** was born in Ma'anshan, China, in 1998. She is currently pursuing the degree in electrical engineering with the China University of Mining and Technology, Beijing, China. Her current research interest includes ac arc fault detection.